7-28-2023

Propagation of Spatiotemporal Optical Vortex Beams in Linear, Second-order Dispersive Media

Milo W. Hyde IV
Air Force Institute of Technolgy

Miguel A. Porras
Grupo de Sistemas Complejos, ETSIME

Recommended Citation

Hyde, M. W., & Porras, M. A. (2023). Propagation of spatiotemporal optical vortex beams in linear, second-order dispersive media. Physical Review A, 108(1), 013519. https://doi.org/10.1103/PhysRevA.108.013519

Propagation of spatiotemporal optical vortex beams in linear, second-order dispersive media

Milo W. Hyde, IV *
Department of Engineering Physics, and Air Force Institute of Technology, Dayton, Ohio 45433, USA

Miguel A. Porras
Grupo de Sistemas Complejos, ETSIME, and Universidad Politécnica de Madrid, Rios Rosas 21, 28003 Madrid, Spain

(Received 21 March 2023; accepted 7 July 2023; published 28 July 2023)

In this paper, we study the behaviors of spatiotemporal optical vortex (STOV) beams propagating in linear dispersive media. Starting with the Fresnel diffraction integral, we derive a closed-form expression for the STOV field at any propagation distance z in a general second-order dispersive medium. We compare our general result to special cases published in the literature and examine the characteristics of higher-order STOV beams propagating in dispersive materials by varying parameters of the medium and source-plane STOV field. We validate our analysis by comparing theoretical predictions to numerical computations of a higher-order STOV beam propagating through fused silica, where we model the index of refraction with the corresponding Sellmeier equation.

DOI: 10.1103/PhysRevA.108.013519

I. INTRODUCTION

Beam shaping or control has traditionally focused on manipulating light either spatially or temporally. However, this has begun to change with the development of space-time-coupled (STC) light beams. As the name implies, STC fields are solutions to Maxwell's equations where space and time are not multiplicatively separable. Although known for quite some time, STC fields and their effects were first observed with the use of femtosecond pulsed lasers and considerable effort has been devoted to modeling and measuring STC [1–6]. In the past few years, attention has turned to controlling STC to create light beams with novel and exploitable traits. Recent examples of STC light include beams whose space-time profiles can be controlled in free-space propagation [7–11], fields that experience anomalous refraction at material interfaces [12–14], and light that is immune to modal dispersion in waveguides [15].

Of all the STC light that has been studied to date [16,17], probably the most popular today are the so-called spatiotemporal optical vortex (STOV) beams. STOV beams possess a phase vortex that couples their space and time dimensions making them the space-time counterparts of traditional vortex fields, such as Laguerre-Gauss (LG) and Bessel-Gauss (BG) beams [18–21]. Like LG and BG light fields, STOV beams carry orbital angular momentum (OAM); in contrast, the OAM direction is transverse to the direction of propagation [22–24]. This peculiarity has made STOV beams quite popular due to their potential uses in optical trapping, atomic optics, and optical communications.

STOV carrying light beams are now routinely generated in the laboratory [24–32] and much effort recently has been dedicated to understanding how these beams evolve as they propagate. Indeed, several recent papers are devoted to this subject [27,29,33–35]. Of these, Refs. [34,35] are the most relevant: In the former, the author derives an expression for the field of a propagated STOV beam of any order in a nondispersive medium. Prior to this work, such an expression had only been obtained for first-order STOV fields [35]; others examined STOV propagation either numerically or experimentally [24,28–30,33]. The authors of Ref. [35] present modal analysis, using spatiotemporal Hermite-Gauss (HG) beams as basis or expansion functions, to study STOV fields in both vacuum and dispersive media. While their modal approach is generally applicable to STOVs of any order [36], the authors analyze only first-order STOV beams. What remains to be found is a single expression for higher-order STOV propagation, like that in Ref. [34], yet applicable in dispersive media (see Ref. [35]). This need becomes more imperative as STOV beams transition from research to applied physics.

In this paper, we derive such an expression. Starting in the temporal frequency ω domain with the Fresnel diffraction integral, we derive the ω-domain field for a propagated higher-order STOV beam applicable in any linear, homogeneous, and isotropic medium. Then, assuming that the STOV source field is narrow band (as in all experiments to date), we Fourier transform the result to obtain the desired time-domain expression. We discuss special cases, including zeroth- (equivalent to a pulsed Gaussian beam) and first-order STOVs as well as nondispersive media, and confirm that our expression simplifies to the corresponding relations in the published literature. In addition, we study, in a manner similar to Ref. [35], how

*milo.hyde@afit.edu

higher-order STOVs behave in dispersive media by varying the group velocity dispersion (GVD) coefficient and the STOV's ellipticity (defined below). Lastly, we validate our analysis computationally by comparing theory to numerical results of a higher-order STOV beam propagating through fused silica, modeling its index of refraction using the Sellmeier equation. We conclude with a brief summary of our work.

II. THEORY

A. Frequency-domain expression

It is convenient to begin the analysis in the temporal frequency ω domain and therefore, we start with the Fresnel diffraction integral [37]:

$$U(\boldsymbol{\rho}, z, \omega) = \frac{\exp(jkz)}{j\lambda z}\exp\left(\frac{jk}{2z}\rho^2\right)\iint_{-\infty}^{\infty} U(\boldsymbol{\rho}', 0, \omega) \times \exp\left(\frac{jk}{2z}\rho'^2\right)\exp\left(-j\frac{k}{z}\boldsymbol{\rho}\cdot\boldsymbol{\rho}'\right)d^2\rho', \quad (1)$$

where $j = \sqrt{-1}$, $\boldsymbol{\rho} = \hat{\mathbf{x}}x + \hat{\mathbf{y}}y$, and k and λ are the wave number and wavelength in the dispersive medium, respectively. The dependence of k on ω is implicit and omitted for brevity.

The $z = 0$ or source-plane field in Eq. (1) is the Fourier transform of the time-domain STOV field, which has the form of a zeroth-order (zero radial index) spatiotemporal LG beam [27,29,34,35], namely,

$$U(\boldsymbol{\rho}', 0, t) = A\exp\left(-\frac{y'^2}{\sigma_y^2}\right)\left[\frac{t}{\sigma_t} + j\,\mathrm{sgn}(\ell)\frac{x'}{\sigma_x}\right]^{|\ell|} \times \exp\left[-\left(\frac{x'^2}{\sigma_x^2} + \frac{t^2}{\sigma_t^2}\right)\right]\exp(-j\omega_c t). \quad (2)$$

Here, A controls the field's amplitude; σ_x, σ_y, and σ_t are the $1/e$ radii of the beam in the x, y, and t dimensions, respectively; ℓ is the topological charge or order of the STOV; $\mathrm{sgn}(x)$ is the signum function; and ω_c is the optical or carrier frequency. We assume a quasimonochromatic regime where the envelope of the STOV field comprises many optical cycles, such that $\sigma_t\omega_c \gg \pi$. This condition is satisfied by all STOV beams generated in the literature to date. For example, in Refs. [24,25,27–30], STOV fields are generated having $\lambda_c \approx 800$ nm ($f_c \approx 375$ THz) and $\sigma_t \approx 50$ fs, making $\sigma_t\omega_c \approx 118 \gg \pi$.

Computing the Fourier transform of Eq. (2), see 3.462.4 in Ref. [38], and substituting the result into Eq. (1) yields

$$U(\boldsymbol{\rho}, z, \omega) = A\frac{\exp(jkz)}{j\lambda z}\exp\left(\frac{jk}{2z}\rho^2\right)\left(\frac{j}{2}\right)^{|\ell|}\frac{\sigma_t}{2\sqrt{\pi}}\exp\left(-\frac{\sigma_t^2}{4}\bar{\omega}^2\right)\int_{-\infty}^{\infty}\exp\left[-\left(1 - j\frac{k\sigma_y^2}{2z}\right)\frac{y'^2}{\sigma_y^2}\right]\exp\left(-j\frac{k}{z}yy'\right)dy' \times \int_{-\infty}^{\infty} H_{|\ell|}\left[\frac{\sigma_t}{2}\bar{\omega} + \mathrm{sgn}(\ell)\frac{x'}{\sigma_x}\right]\exp\left[-\left(1 - j\frac{k\sigma_x^2}{2z}\right)\frac{x'^2}{\sigma_x^2}\right]\exp\left(-j\frac{k}{z}xx'\right)dx', \quad (3)$$

where $\bar{\omega} = \omega - \omega_c$ and $H_{|\ell|}(x)$ is an $|\ell|$th-order Hermite polynomial [38,39]. We now make the substitutions $u' = x'/\sigma_x$ and $v' = y'/\sigma_y$ (likewise for the observation coordinates $u = x/\sigma_x$ and $v = y/\sigma_y$) and recognize that $N_{Fx} = k\sigma_x^2/(2z)$ and $N_{Fy} = k\sigma_y^2/(2z)$ are the Fresnel numbers in the x and y directions, respectively; these transform Eq. (3) into

$$U(\boldsymbol{\rho}, z, \omega) = A\frac{\exp(jkz)}{j\lambda z}\left(\frac{j}{2}\right)^{|\ell|}\frac{\sigma_t}{2\sqrt{\pi}}\exp\left(-\frac{\sigma_t^2}{4}\bar{\omega}^2\right)\sigma_y\exp(jN_{Fy}v^2)\int_{-\infty}^{\infty}\exp[-(1 - jN_{Fy})v'^2]\exp(-j2N_{Fy}vv')dv' \times \sigma_x\exp(jN_{Fx}u^2)\int_{-\infty}^{\infty} H_{|\ell|}\left[\frac{\sigma_t}{2}\bar{\omega} + \mathrm{sgn}(\ell)u'\right]\exp[-(1 - jN_{Fx})u'^2]\exp(-j2N_{Fx}uu')du'. \quad (4)$$

Both integrals can be evaluated in closed form, the latter by making the substitution $\psi = \sigma_t\bar{\omega}/2 + \mathrm{sgn}(\ell)u'$, completing the square of the resulting exponential's argument, and finally applying 7.374.10 in Ref. [38]. The result, after some effort, is

$$U(\boldsymbol{\rho}, z, \omega) = A\frac{\sigma_t}{2\sqrt{\pi}}\exp(jkz)\exp\left(-\frac{\sigma_t^2}{4}\bar{\omega}^2\right)\sqrt{\frac{-jN_{Fx}}{1 - jN_{Fx}}}\exp\left(\frac{jN_{Fx}}{1 - jN_{Fx}}u^2\right)\sqrt{\frac{-jN_{Fy}}{1 - jN_{Fy}}}\exp\left(\frac{jN_{Fy}}{1 - jN_{Fy}}v^2\right) \times \left(\frac{j}{2}\right)^{|\ell|}\left(\frac{-jN_{Fx}}{1 - jN_{Fx}}\right)^{|\ell|/2} H_{|\ell|}\left[\frac{\sigma_t}{2}\sqrt{\frac{1 - jN_{Fx}}{-jN_{Fx}}}\bar{\omega} + \mathrm{sgn}(\ell)\sqrt{\frac{-jN_{Fx}}{1 - jN_{Fx}}}u\right]. \quad (5)$$

B. Time-domain expression

Equation (5) is the frequency-domain field for a STOV beam propagated to any location z. To obtain the time-domain field, we must inverse Fourier transform Eq. (5), which is generally not possible because of the nonlinear ω dependence of k. However, since our STOV field is narrow band (recall $\sigma_t\omega_c \gg \pi$), we can expand k in a Taylor series about ω_c and retain only the first three terms, such that

$$k(\omega) \approx k(\omega_c) + k'(\omega_c)\bar{\omega} + k''(\omega_c)\frac{\bar{\omega}^2}{2}, \quad (6)$$

where $k(\omega_c)$, $k'(\omega_c)$, and $k''(\omega_c)$. denoted as k_c, k_c', and k_c'' hereafter, are the traditional wave number $k_c = \omega_c/v_p$ (v_p is the phase velocity), inverse group velocity $k_c' = 1/v_g$, and

GVD coefficient at ω_c, respectively. Substituting Eq. (6) into Eq. (5), approximating $N_{F\alpha} \approx k_c^2\sigma_\alpha^2/(2z)$ (i.e., diffraction's dependence on $\bar{\omega}$ is negligible over the STOV's bandwidth), and inverse Fourier transforming the result produces

$$U(\boldsymbol{\rho},z,t) \approx A\frac{\sigma_t}{2\sqrt{\pi}}\exp\left[-j(\omega_c t-k_c z)\right]\left(\frac{j}{2}\right)^{|\ell|}\sqrt{\frac{z_{Ry}}{jq_y}}\exp\left(j\frac{z_{Ry}}{q_y}v^2\right)\sqrt{\frac{z_{Rx}}{jq_x}}\exp\left(j\frac{z_{Rx}}{q_x}u^2\right)$$
$$\times\left(\frac{z_{Rx}}{jq_x}\right)^{|\ell|/2}\int_{-\infty}^{\infty}H_{|\ell|}\left[\sqrt{\frac{jq_x}{z_{Rx}}}\frac{\sigma_t}{2}\bar{\omega}+\operatorname{sgn}(\ell)\sqrt{\frac{z_{Rx}}{jq_x}}u\right]\exp\left(-\frac{\sigma''\sigma_t^2}{4}\bar{\omega}^2\right)\exp(-j\bar{\omega}\tau)d\bar{\omega}, \tag{7}$$

where $z_{R\alpha}=k_c^2\sigma_\alpha^2/2$ ($\alpha=x,y$) is the Rayleigh range and $q_\alpha=z-jz_{R\alpha}$ is the complex Gaussian beam parameter. In addition, $\tau=t-k_c'z$ is the retarded time and $\sigma''=1-j\operatorname{sgn}(k_c'')z/z_D$, where $z_D=\sigma_t^2/(2|k_c''|)$ is the dispersion length. The remaining integral in Eq. (7) can be evaluated using the same procedure that led to Eq. (5); the final result is

$$U(\boldsymbol{\rho},z,t)=U_e(\boldsymbol{\rho},z,t)\exp\left[-j(\omega_c t-k_c z)\right]$$
$$U_e(\boldsymbol{\rho},z,t)=\frac{A}{j}\sqrt{\frac{z_{Rx}z_{Ry}}{q_xq_y}}\exp\left(j\frac{k_cx^2}{2q_x}\right)\exp\left(j\frac{k_cy^2}{2q_y}\right)\sqrt{\frac{1}{\sigma''}}\exp\left(-\frac{\tau^2}{\sigma''\sigma_t^2}\right)\left(\frac{1}{\sigma''}+j\frac{z_{Rx}}{q_x}\right)^{|\ell|/2}$$
$$\times\frac{1}{2^{|\ell|}}H_{|\ell|}\left[\left(\frac{1}{\sigma''}+j\frac{z_{Rx}}{q_x}\right)^{-\frac{1}{2}}\left(\frac{\tau}{\sigma''\sigma_t}+\operatorname{sgn}(\ell)\frac{z_{Rx}}{q_x}\frac{x}{\sigma_x}\right)\right]. \tag{8}$$

Equation (8) is the main theoretical result of this paper, and there are a few aspects of the expression worth noting:

(i) When $\ell=0$, Eq. (8) simplifies to the expression for a pulsed Gaussian beam propagating in a dispersive medium [40–43]. The exponentials in U_e are the spatial and temporal envelopes, respectively. Both have Gaussian amplitudes and chirped phases. In the former, the phase is up chirped, modeling a spatially diverging wavefront; whereas, in the latter, the chirp is either up or down depending on the sign of k_c''. The unitless dispersion parameter σ'' is ultimately responsible for pulse broadening and temporal chirping.

(ii) In a nondispersive medium, $v_g=v_p$, $\sigma''=1$, and Eq. (8) reduces to Eq. (7) in Ref. [34].

(iii) For a first-order ($\ell=\pm1$) STOV beam, it is relatively easy to show, by applying the summation theorem for Hermite polynomials (8.958.1 in Ref. [38]), that Eq. (8) is equivalent to Eq. (7) in Ref. [35]. Indeed, we can use that theorem to write Eq. (8) as a sum of HG beams for any ℓ, in effect, generalizing the first-order result in Ref. [35]. Applying 8.958.1 in Ref. [38], Eq. (8) becomes

$$U_e(\boldsymbol{\rho},z,t)=Ah_0^y(y,z)\sum_{i+j=|\ell|}h_i^x(x,z)h_j^t(t,z), \tag{9}$$

where h_i^x and h_j^t are

$$h_i^x(x,z)=[j\operatorname{sgn}(\ell)]^i\sqrt{\frac{|\ell|!}{2^{|\ell|}}}\frac{1}{i!}\left(\sqrt{\frac{z_{Rx}}{jq_x}}\right)^{i+1}$$
$$\times\exp\left(j\frac{z_{Rx}}{q_x}\frac{x^2}{\sigma_x^2}\right)H_i\left(\sqrt{\frac{z_{Rx}}{jq_x}}\frac{x}{\sigma_x}\right),$$
$$h_j^t(t,z)=\sqrt{\frac{|\ell|!}{2^{|\ell|}}}\frac{1}{j!}\left(\frac{1}{\sqrt{\sigma''}}\right)^{j+1}$$
$$\times\exp\left(-\frac{\tau^2}{\sigma''\sigma_t^2}\right)H_j\left(\frac{\tau}{\sqrt{\sigma''}\sigma_t}\right). \tag{10}$$

The function h_0^y is of the exact same form as h_i^x, just with y replacing x. We note that Eq. (9) is expanded in terms of elegant HG beams [19], vice the standard modes used in Ref. [35].

(iv) Lastly, in the far zone $z_{R\alpha}/q_\alpha \sim z_{R\alpha}/z+j(z_{R\alpha}/z)^2$, which simplifies Eq. (8) to

$$U_e(\boldsymbol{\rho},z,t)\sim A\sqrt{\frac{1}{\sigma''}}\exp\left(-\frac{\tau^2}{\sigma''\sigma_t^2}\right)$$
$$\times\frac{\sqrt{z_{Rx}z_{Ry}}}{jz}\exp\left(j\frac{k_c}{2z}\rho^2\right)\exp\left[-\left(\frac{\theta_x^2}{\theta_{0x}^2}+\frac{\theta_y^2}{\theta_{0y}^2}\right)\right]$$
$$\times\left(\frac{1}{2\sqrt{\sigma''}}\right)^{|\ell|}H_{|\ell|}\left[\sqrt{\sigma''}\left(\frac{\tau}{\sigma''\sigma_t}+\operatorname{sgn}(\ell)\frac{\theta_x}{\theta_{0x}}\right)\right], \tag{11}$$

where $\theta_\alpha=\alpha/z$ and $\theta_{0\alpha}=\sigma_\alpha/z_{R\alpha}$ are the observation and divergence angles, respectively.

C. Discussion

To investigate the behaviors of higher-order STOV beams propagating in dispersive media, we predicted the space-time profiles of the field's envelope, i.e., $U_e(x,0,z,t)$, using Eq. (8) at multiple GVD coefficients, STOV ellipticities, and propagation distances. The results are shown in Figs. 1 and 2, the organization of which is similar to figures presented in Refs. [34,35]: Each figure consists of a 5×3 grid of images; each element of the grid shows the magnitude (top) and phase (bottom) of the propagated U_e. Both the retarded time τ (abscissa) and space x (ordinate) axes are normalized by the pulse and beam radii, i.e., $\sigma_t(z)=\sigma_t\sqrt{1+(z/z_D)^2}$ and $\sigma_x(z)=\sigma_x\sqrt{1+(z/z_{Rx})^2}$, respectively. Row-wise, the images show how the field's envelope varies versus normalized GVD coefficient $\hat{k}_c''=k_c''(k_c/k_c'^2)$, the values of which are given as row headings. The normalized GVD coefficient, in combination with the STOV ellipticity $\gamma=v_g\sigma_t/\sigma_x=\sigma_t/(k_c'\sigma_x)$, relates z_D and z_{Rx}, such that $z_D/z_{Rx}=\gamma^2/|\hat{k}_c''|$. Negative values of $\hat{k}_c''$ imply anomalous dispersion, $\hat{k}_c''=0$ is a nondispersive

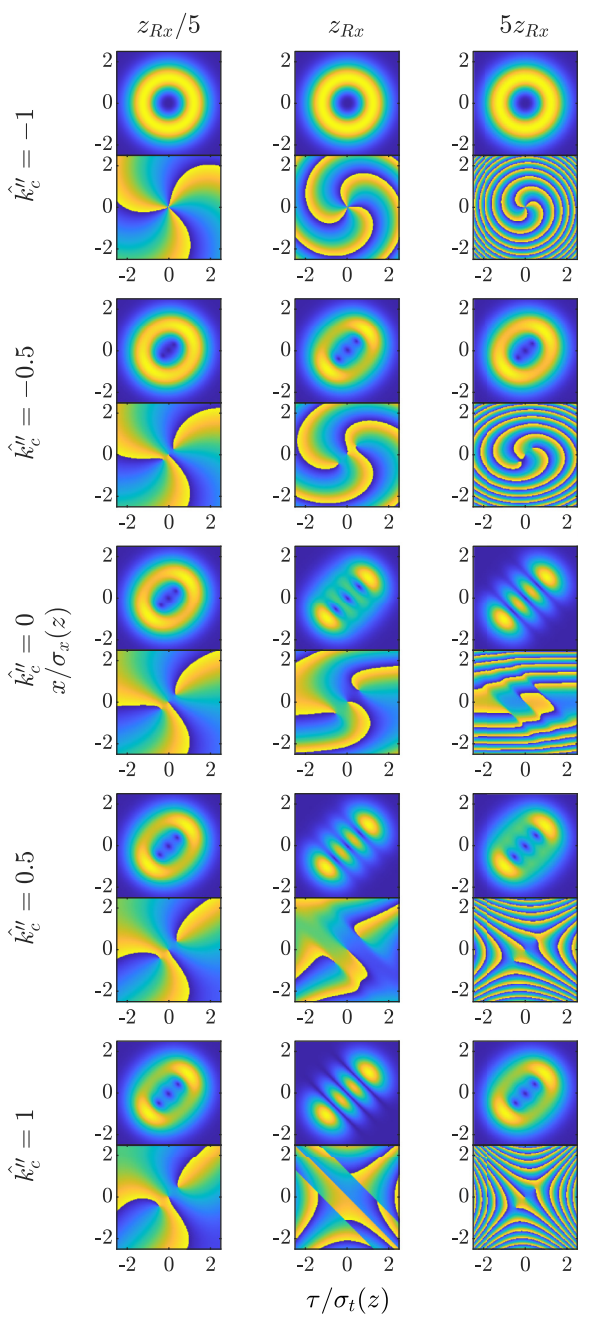

FIG. 1. Space-time profiles of a propagated third-order ($\ell = 3$) STOV beam [$U_e(x, 0, z, t)$ in Eq. (8)] with ellipticity $\gamma = \sigma_t/(k_c'\sigma_x) = 1$. The normalized GVD coefficients $\hat{k}_c'' = k_c''(k_c/k_c'^2)$ and propagation distances z are given as row and column headings, respectively. The top and bottom images in each 2×1 group are $|U_e|$ and $\arg(U_e)$.

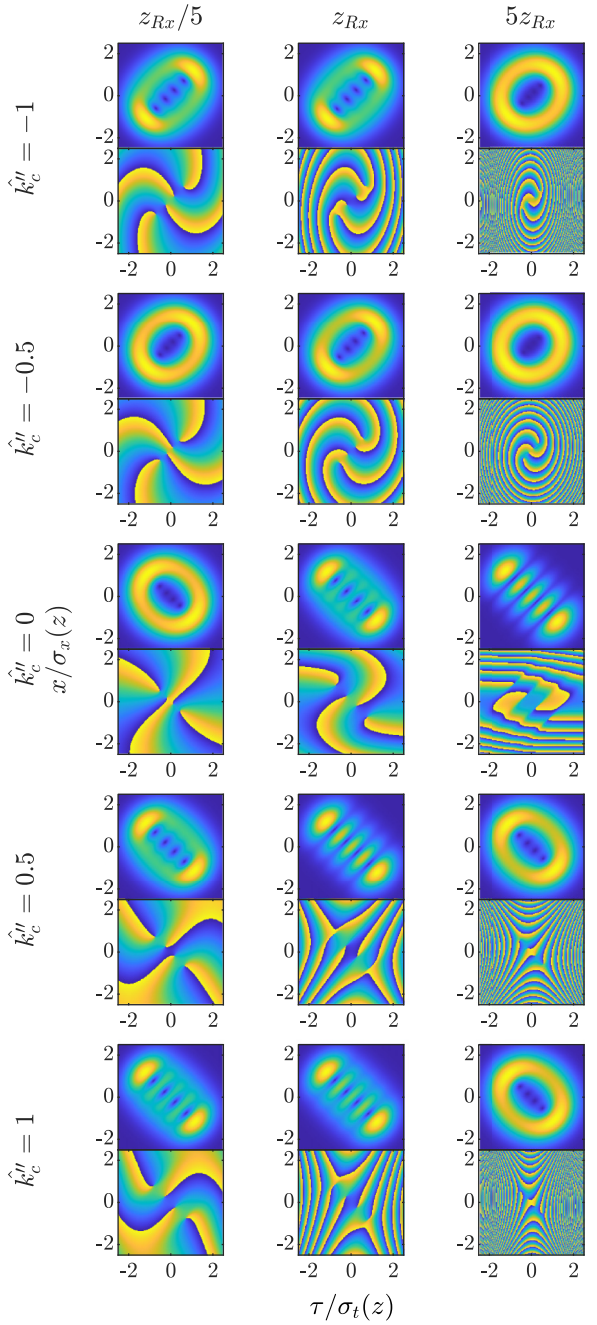

FIG. 2. Space-time profiles of a propagated fourth-order ($\ell = -4$) STOV beam [$U_e(x, 0, z, t)$ in Eq. (8)] with ellipticity $\gamma = \sigma_t/(k_c'\sigma_x) = 0.5$. The normalized GVD coefficients $\hat{k}_c'' = k_c''(k_c/k_c'^2)$ and propagation distances z are given as row and column headings, respectively. The top and bottom images in each 2×1 group are $|U_e|$ and $\arg(U_e)$.

medium, and lastly, $\hat{k}_c'' > 0$ is normal dispersion. The columns in the figures correspond to propagation distances, reported as multiples of the Rayleigh range z_{Rx}. Figure 1 shows the results for a third-order ($\ell = 3$) STOV beam with an ellipticity $\gamma = 1$, i.e., an initially circular STOV beam in the x-$v_g t$ plane. Lastly, Fig. 2 displays the same results as Fig. 1; however, this time for a fourth-order ($\ell = -4$) STOV beam with a $\gamma = 0.5$.

Inspection of Figs. 1 and 2 reveals that the behaviors of multiorder STOV fields in dispersive media are generally similar to $\ell = 1$ beams (see Fig. 2 in Ref. [35]). In particular, the orientations of the STOV ellipses for a specific γ and $\hat{k}_c''$ are identical. Also, the direction of phase circulation around a vortex or phase singularity is the same. This direction can clearly be seen in the phase images. Take for instance, the images for $\hat{k}_c'' = -1$ in Fig. 1, i.e., the first row of the figure: For $z = z_{Rx}/5$, the third-order vortex is clearly visible in the phase image, and the direction of circulation is counterclockwise (i.e., positive charge). As the beam propagates, the $\ell = 3$

vortex and its charge are maintained. This is an expected result, as STOV beams (spatiotemporal LG beams, more generally) are solutions to the space-time paraxial wave equation in media with anomalous dispersion [22,23,25,30]. Consequently, they maintain their shape in such media, if diffraction and dispersion are equal, viz., $z_{Rx} = z_D$. Recently, this behavior has been experimentally confirmed [28,30]. For the other cases of anomalous dispersion ($\gamma \neq 1$ or $0 > \hat{k}_c'' > -1$), the multiorder vortex generally splits into first-order vortices, with the charges remaining the same (positive in Fig. 1 and negative in Fig. 2).

In nondispersive and normally dispersive media, the initial multiorder vortex splits into $\ell = \pm 1$ vortices due to the asymmetry between diffraction and dispersion, a phenomenon called space-time astigmatism. Indeed, one can clearly see this astigmatism in the last row and last column phase images in Figs. 1 and 2. For nondispersive media in particular, space-time astigmatism eventually (in the far zone) leads to the $\ell = \pm 1$ vortices being stretched into parallel lines (π phase jumps) oriented in the direction of the zeros of what ultimately becomes an ℓth-order Hermite polynomial, see Eq. (11) and the phase images for $\hat{k}_c'' = 0$ and $z = 5z_{Rx}$ in Figs. 1 and 2. Since the vortices are now π phase steps corresponding to the zero crossings of the Hermite polynomial, phase circulation ceases. Nevertheless, until the field's envelope assumes its asymptotic far-zone form, the vortex charges are maintained (again, positive in Fig. 1 and negative in Fig. 2). This behavior was reported and analyzed in Ref. [34].

In contrast, for normally dispersive media, the vortices can reverse polarity [22,23]. This is most evident in the last row of Fig. 1, where at $z = z_{Rx}/5$ three positively charged vortices are clearly present. At $z = z_{Rx}$, the vortices have transitioned to three π phase steps. Finally, at $z = 5z_{Rx}$, we again observe three $\ell = 1$ vortices; however, they are now negatively charged. We see the same charge reversal in the corresponding images in Fig. 2.

It should be noted that for $\gamma = 1$, $\hat{k}_c'' = 1$, and $z = z_{Rx}$ (row five and column two of Fig. 1), we obtain a U_e that is essentially equivalent to the far-zone U_e in nondispersive media, with the only differences being the spatial and temporal chirps. We can derive the condition for this equivalence by setting $1/\sigma'' = z_{Rx}/q_x$ and substituting $z_D = z_{Rx}\gamma^2/\hat{k}_c''$. The result is simply $\hat{k}_c'' = \gamma^2$ implying that $z_{Rx} = z_D$. As discussed above, when this condition is met in media with anomalous dispersion, the STOV's shape is preserved during propagation, exactly like the images in the first row of Fig. 1.

III. NUMERICAL VALIDATION

In this section, we analyze numerical results of a higher-order STOV beam propagating through fused silica. Before presenting and comparing those results to predictions using Eq. (8), we briefly discuss the details of the numerical computation.

A. Setup

The starting point for the numerical analysis was the ω-domain propagation expression given in Eq. (5), which we evaluated at multiple z and then inverse fast Fourier transformed (FFT). The STOV beam in the source plane had the following parameter values: $\lambda_c = 800$ nm, $A = 1$, $\ell = -5$, $\sigma_x = \sigma_y = 0.5$ mm, and $\sigma_t = 50$ fs. We discretized the space-frequency (x-$\bar{\omega}$) domain STOV field using $N_x \times N_\omega = 13,262 \times 13,262$ points with grid spacings equal to $\Delta_\omega = 0.127$ THz and $\Delta_x = 0.954$ μm, respectively. The FFT linked the $\bar{\omega}$- and t-domain grids, such that $\Delta_t = 2\pi/(N_\omega \Delta_\omega) = 3.74$ fs and $L_t = N_\omega \Delta_t = 49.5$ ps.

For Eq. (5), we computed the wave number $k = \omega n(\omega)/c$ and Fresnel number $N_{F\alpha}$ over the 13,262-point ω grid (i.e., the $\bar{\omega}$ grid described above centered at ω_c) using the fused silica Sellmeier equation for the index of refraction $n(\omega)$ published in Ref. [44]. Applying that relation at $\lambda_c = 800$ nm, the k_c, k_c', and k_c'' used in the theoretical expression Eq. (8) were 11.414 rad/μm, 4.894 fs/μm, and 0.036163 fs^2/μm, respectively. These, when combined with the σ_t and σ_x listed above, made the ellipticity and normalized GVD coefficient equal to $\gamma = 0.0204$ and $\hat{k}_c'' = 0.0172$.

Lastly, the propagation distances in the numerical solutions were $z = z_D/5$, z_D, $5z_D$, $10z_D$, $20z_D$, z_{Rx}, and $3z_{Rx}$ ($z_{Rx} \approx 40z_D$). We have also included a 40 s animation as Supplemental Material, which shows the evolution of the STOV beam in fused silica in steps of $\Delta_z \approx z_D/5$ over the same $z \in [z_D/5, 3z_{Rx}]$ range [45].

B. Results

Figure 3 shows the results and is organized as follows. Figure 3(a) is composed of two rows and six columns of 2×1 images. The first and second rows show the theoretical [computed using Eq. (8)] and numerical $U_e(x, 0, z, t)$, while the columns, from left to right, display the U_e for increasing z—the values of which are provided as column headings. Like in Figs. 1 and 2, $|U_e|$ and $\arg(U_e)$ are the top and bottom images in each 2×1 element comprising Fig. 3(a). In addition, the theoretical and numerical $|U_e|$ at each z are plotted using the same color scale. Figure 3(b) directly compares theory and the numerical results by plotting the diagonal slices through the $|U_e|$ in Fig. 3(a). The theoretical and numerical results are the solid-blue and dashed-red traces, respectively.

Overall, the theoretical and numerical results are in excellent accord. The quality of these results validates our analysis in Sec. II. Note that in Fig. 3(a) we observe repeating $|U_e|$, just like in Figs. 1 and 2. Indeed, aside from physical size and amplitude values, the $|U_e|$ at $z = z_D$ and z_{Rx} are effectively equivalent. In addition, the $|U_e|$ at $z = 5z_D \approx z_{Rx}/8$ and $z = 10z_D \approx z_{Rx}/4$ (i.e., the temporal far zone) are very similar to the far zone $|U_e|$ for an $\ell = -5$ STOV beam in nondispersive media.

IV. CONCLUSION

In this paper, we derived a closed-form expression for the STOV field of any order, at any propagation distance z, in a second-order dispersive medium. We then analyzed our general result by comparing it to special cases in the literature and examined STOV beam behavior in dispersive media by varying both the initial STOV's ellipticity and the GVD coefficient of the medium. We validated our

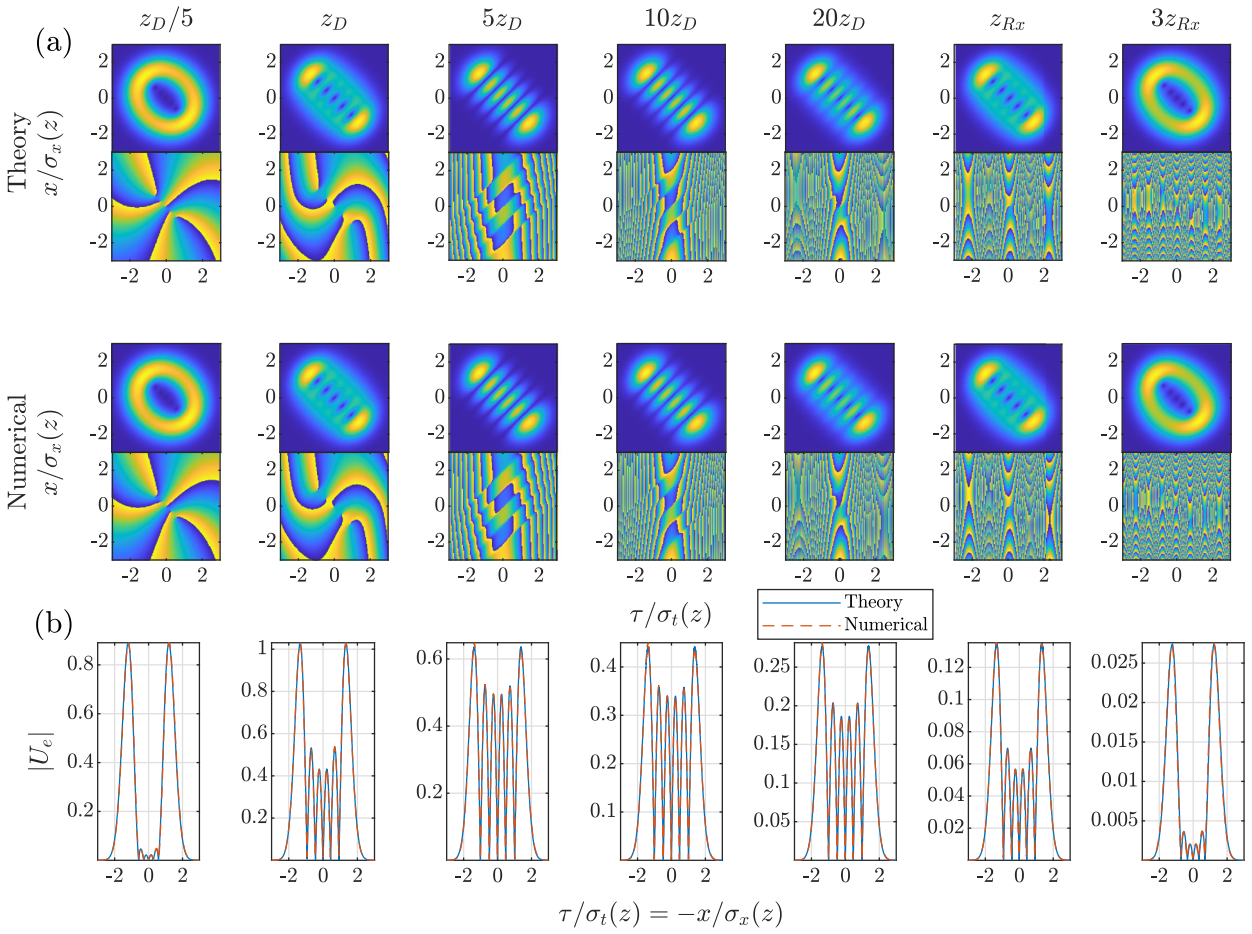

FIG. 3. Numerical results of a fifth-order, negatively charged STOV beam propagating through fused silica. (a) The top and bottom rows of 2×1 figures show the theoretical and numerical results, with $|U_e(x, 0, z, t)|$ and $\arg[U_e(x, 0, z, t)]$ displayed as the top and bottom images, respectively. The theoretical and numerical $|U_e|$ at each propagation distance z are plotted using the same color scale. (b) Diagonal slices through the theoretical and numerical $|U_e|$ in (a).

theoretical result computationally by inverse Fourier transforming (i.e., inverse FFT) the frequency domain expression for a fifth-order, negatively charged STOV beam propagating through fused silica, modeling the index of refraction over the STOV's bandwidth using the Sellmeier equation. We compared the numerical STOV field results to those predicted by our analytical expression and found them to be in excellent agreement.

STOV beams and space-time-coupled fields, more generally, are new and exciting advancements in beam control research with many potential applications. Our work, which predicts how STOV-carrying light behaves in general linear media, is a necessary step in ultimately applying these structured light fields.

ACKNOWLEDGMENTS

M.A.P. acknowledges support of the Spanish Ministry of Science and Innovation, Gobierno de España, under Contract No. PID2021-122711NB-C21. The views expressed in this paper are those of the authors and do not reflect the official policy or position of the US Air Force, the Department of Defense, or the US government.

[1] S. Akturk, X. Gu, P. Gabolde, and R. Trebino, The general theory of first-order spatio-temporal distortions of Gaussian pulses and beams, Opt. Express **13**, 8642 (2005).

[2] P. Gabolde, D. Lee, S. Akturk, and R. Trebino, Describing first-order spatio-temporal distortions in ultrashort pulses using normalized parameters, Opt. Express **15**, 242 (2007).

[3] S. Akturk, X. Gu, P. Bowlan, and R. Trebino, Spatio-temporal couplings in ultrashort laser pulses, J. Opt. **12**, 093001 (2010).

[4] S. W. Jolly, O. Gobert, and F. Quéré, Spatio-temporal characterization of ultrashort laser beams: A tutorial, J. Opt. **22**, 103501 (2020).

[5] R. Trebino, P. Bowlan, P. Gabolde, X. Gu, S. Akturk, and M. Kimmel, Simple devices for measuring complex ultrashort pulses, Laser and Photon. Rev. **3**, 314 (2009).

[6] R. Trebino, R. Jafari, S. A. Akturk, P. Bowlan, Z. Guang, P. Zhu, E. Escoto, and G. Steinmeyer, Highly reliable measurement of ultrashort laser pulses, J. Appl. Phys. **128**, 171103 (2020).

[7] J. C. Vaughan, T. Feurer, and K. A. Nelson, Automated two-dimensional femtosecond pulse shaping, J. Opt. Soc. Am. B **19**, 2489 (2002).

[8] J. C. Vaughan, T. Feurer, and K. A. Nelson, Automated spatiotemporal diffraction of ultrashort laser pulses, Opt. Lett. **28**, 2408 (2003).

[9] J. C. Vaughan, T. Hornung, T. Feurer, and K. A. Nelson, Diffraction-based femtosecond pulse shaping with a two-dimensional spatial light modulator, Opt. Lett. **30**, 323 (2005).

[10] H. E. Kondakci and A. F. Abouraddy, Diffraction-free pulsed optical beams via space-time correlations, Opt. Express **24**, 28659 (2016).

[11] H. E. Kondakci and A. F. Abouraddy, Diffraction-free space-time light sheets, Nature Photon. **11**, 733 (2017).

[12] M. Yessenov, B. Bhaduri, and A. F. Abouraddy, Refraction of space-time wave packets: I. Theoretical principles, J. Opt. Soc. Am. A **38**, 1409 (2021).

[13] A. M. Allende Motz, M. Yessenov, B. Bhaduri, and A. F. Abouraddy, Refraction of space-time wave packets: II. Experiments at normal incidence, J. Opt. Soc. Am. A **38**, 1450 (2021).

[14] M. Yessenov, A. M. Allende Motz, B. Bhaduri, and A. F. Abouraddy, Refraction of space-time wave packets: III. Experiments at oblique incidence, J. Opt. Soc. Am. A **38**, 1462 (2021).

[15] A. Shiri, S. Webster, K. L. Schepler, and A. F. Abouraddy, Propagation-invariant space-time supermodes in a multimode waveguide, Optica **9**, 913 (2022).

[16] M. Yessenov, L. A. Hall, K. L. Schepler, and A. F. Abouraddy, Space-time wave packets, Adv. Opt. Photon. **14**, 455 (2022).

[17] Y. Shen, Q. Zhan, L. G. Wright, D. N. Christodoulides, F. W. Wise, A. Willner, K. Zou, Z. Zhao, M. A. Porras, A. Chong, C. Wan, K. Y. Bliokh, C.-T. Liao, C. H. Garcia, M. M. Murnane, M. Yessenov, A. Abouraddy, L. J. Wong, M. Go, S. Kumar *et al.*, Roadmap on spatiotemporal light fields, J. Opt. (2023), doi:10.1088/2040-8986/ace4dc.

[18] H. Kogelnik and T. Li, Laser beams and resonators, Proc. IEEE **54**, 1312 (1966).

[19] A. E. Siegman, *Lasers* (University Science Books, Palo Alto, 1986).

[20] F. Gori, G. Guattari, and C. Padovani, Bessel-Gauss beams, Opt. Commun. **64**, 491 (1987).

[21] U. Levy, S. Derevyanko, and Y. Silberberg, Light modes of free space, in *Progress in Optics*, Vol. 61, edited by T. D. Visser (Elsevier, Amsterdam, 2016), Chap. 4, pp. 237–281.

[22] K. Y. Bliokh and F. Nori, Spatiotemporal vortex beams and angular momentum, Phys. Rev. A **86**, 033824 (2012).

[23] K. Y. Bliokh, Spatiotemporal Vortex Pulses: Angular Momenta and Spin-Orbit Interaction, Phys. Rev. Lett. **126**, 243601 (2021).

[24] A. Chong, C. Wan, J. Chen, and Q. Zhan, Generation of spatiotemporal optical vortices with controllable transverse orbital angular momentum, Nature Photon. **14**, 350 (2020).

[25] M. Dallaire, N. McCarthy, and M. Piché, Spatiotemporal Bessel beams: Theory and experiments, Opt. Express **17**, 18148 (2009).

[26] N. Jhajj, I. Larkin, E. W. Rosenthal, S. Zahedpour, J. K. Wahlstrand, and H. M. Milchberg, Spatiotemporal Optical Vortices, Phys. Rev. X **6**, 031037 (2016).

[27] S. W. Hancock, S. Zahedpour, A. Goffin, and H. M. Milchberg, Free-space propagation of spatiotemporal optical vortices, Optica **6**, 1547 (2019).

[28] W. Chen, W. Zhang, Y. Liu, F.-C. Meng, J. M. Dudley, and Y.-Q. Lu, Time diffraction-free transverse orbital angular momentum beams, Nature Commun. **13**, 4021 (2022).

[29] S. Huang, P. Wang, X. Shen, J. Liu, and R. Li, Diffraction properties of light with transverse orbital angular momentum, Optica **9**, 469 (2022).

[30] Q. Cao, J. Chen, K. Lu, C. Wan, A. Chong, and Q. Zhan, Non-spreading Bessel spatiotemporal optical vortices, Sci. Bull. **67**, 133 (2022).

[31] Q. Cao, J. Chen, K. Lu, C. Wan, A. Chong, and Q. Zhan, Sculpturing spatiotemporal wavepackets with chirped pulses, Photon. Res. **9**, 2261 (2021).

[32] L. Chen, W. Zhu, P. Huo, J. Song, H. J. Lezec, T. Xu, and A. Agrawal, Synthesizing ultrafast optical pulses with arbitrary spatiotemporal control, Sci. Adv. **8**, eabq8314 (2022).

[33] S. Huang, P. Wang, X. Shen, and J. Liu, Properties of the generation and propagation of spatiotemporal optical vortices, Opt. Express **29**, 26995 (2021).

[34] M. A. Porras, Propagation of higher-order spatiotemporal vortices, Opt. Lett. **48**, 367 (2023).

[35] S. W. Hancock, S. Zahedpour, and H. M. Milchberg, Mode Structure and Orbital Angular Momentum of Spatiotemporal Optical Vortex Pulses, Phys. Rev. Lett. **127**, 193901 (2021).

[36] Using the modal approach in Ref. [35] requires that one find the weights of the spatiotemporal HG beams that comprise the STOV source field.

[37] J. W. Goodman, *Introduction to Fourier Optics*, 4th ed. (W. H. Freeman and Company, New York, 2017).

[38] I. S. Gradshteyn and I. M. Ryzhik, *Table of Integrals, Series, and Products*, 7th ed., edited by A. Jeffrey and D. Zwillinger (Academic Press, New York, 2007).

[39] M. Abramowitz and I. A. Stegun, eds., *Handbook of Mathematical Functions With Formulas, Graphs, and Mathematical Tables* (National Bureau of Standards, Washington, DC, 1964).

[40] M. A. Porras, Propagation of single-cycle pulsed light beams in dispersive media, Phys. Rev. A **60**, 5069 (1999).

[41] Q. Lin and E. Wintner, Three-dimensional evolution of ultrashort pulses in dispersive media beyond the slowly varying envelope approximation, Opt. Commun. **150**, 185 (1998).

[42] G. P. Agrawal, Far-field diffraction of pulsed optical beams in dispersive media, Opt. Commun. **167**, 15 (1999).

[43] L. Zhi-Jun and L. Bai-Da, Propagation of ultrashort pulsed beams in dispersive media, Chin. Phys. **12**, 879 (2003).

[44] I. H. Malitson, Interspecimen comparison of the refractive index of fused silica, J. Opt. Soc. Am. **55**, 1205 (1965).

[45] See Supplemental Material at http://link.aps.org/supplemental/10.1103/PhysRevA.108.013519 for the animation of a fifth-order, negatively charged STOV beam propagating in fused silica.